Seismic response of fractures and induced anisotropy in poroelastic media

SEG Rock Physics Workshop, Quindao, October 25-27, 2019

Juan E. Santos

Instituto del Gas y del Petróleo (IGPUBA), Universidad de Buenos Aires (UBA), Argentina, Department of Mathematics, Purdue University, West Lafayette, Indiana, USA,

.

October 25, 2019

Seismic waves in fractured fluid-saturated poroelastic materials.

- A planar fracture embedded in a fluid-saturated poroelastic – Biot - medium can be modeled as a extremely thin, highly permeable and compliant porous layer.
- A Biot medium containing a dense set of aligned fractures behaves as an effective viscoelastic transversely isotropic medium (VTI) when the average fracture distance is much smaller than the predominant wavelength of the traveling waves.
- This leads to frequency and angular variations of velocity and attenuation of seismic waves.

Seismic waves in fractured fluid-saturated poroelastic materials. II

- P-waves traveling in this type of medium induce fluid-pressure gradients at fractures and mesoscopic-scale heterogeneities, generating fluid flow and slow (diffusion) Biot waves, causing attenuation and dispersion of the fast modes (mesoscopic loss).
- A poroelastic medium with embedded aligned fractures exhibits significant attenuation and dispersion effects due to this mechanism.
- Due to the extremely fine meshes needed to properly represent these mesoscopic-scale fractures, numerical simulations are very expensive or even not feasible.

Seismic waves in fractured fluid-saturated poroelastic materials. III

- Our approach: In the context of Numerical Rock Physics, we use a numerical upscaling procedure to determine the complex and frequency dependent stiffness at the macroscale of a VTI medium equivalent to a Biot medium with aligned fractures.
- To determine the complex stiffness coefficients of the equivalent VTI medium at the macroscale, we solve a set of boundary value problems (BVP's) for Biot's equation in the diffusive range.
- The BVP's are stated and solved in the space-frequency-domain using the finite-element method (FEM).

Seismic waves in fractured fluid-saturated poroelastic materials. IV

- The BVP's represent harmonic tests at a finite number of frequencies on a representative sample of the material.
- Numerical Rock Physics offer an alternative to laboratory measurements.
- Numerical experiments are inexpensive and informative since the physical process of wave propagation can be inspected during the experiment.
- Moreover, they are repeatable, essentially free from experimental errors, and may easily be run using alternative models of the rock and fluid properties.

The Mesoscale. Anisotropic poroelasticity. I

- For Biot's media, White et al. (1975) were the first to introduce the mesoscopic-loss mechanism in the framework of Biot's theory.
- For fine layered poroelastic materials, the theories of Gelinsky and Shapiro (GPY, 62, 1997) and Krzikalla and Müller (GPY, 76, 2011) allow to obtain the five complex and frequency-dependent stiffnesses of the equivalent VTI medium.
- To provide a more general modeling tool, we present a numerical upscaling procedure to obtain the complex stiffnesses of the effective VTI medium.

The Mesoscale. Anisotropic poroelasticity. II

- We employ the FEM to solve in the space-frequency domain Biot's equations in the diffusive range with boundary conditions representing compressibility and shear harmonic experiments.

- The methodology is applied to saturated isotropic poroelastic samples having a dense set of horizontal fractures.

- The samples contained mesoscopic-scale heterogeneities due to patchy brine-CO_2 saturation and fractal porosity and consequently, fractal permeability and frame properties.

The Mesoscale. Anisotropic poroelasticity. III

Consider isotropic fluid-saturated poroelastic layers.
$u^s(x), u^f(x)$ **: time Fourier transform of the displacement vector of the solid and fluid relative to the solid frame, respectively.**

$u = (u^s, u^f)$

$\sigma_{kl}(u), p_f(u)$**: Fourier transform of the total stress and the fluid pressure, respectively**

On each plane layer n in a sequence of N layers, the frequency-domain stress-strain relations are

$$\sigma_{kl}(u) = 2\mu\, \varepsilon_{kl}(u^s) + \delta_{kl}\left(\lambda_G \nabla \cdot u^s + \alpha M \nabla \cdot u^f\right),$$

$$\mathbf{p}_f(u) = -\alpha M \nabla \cdot u^s - M \nabla \cdot u^f .$$

The Mesoscale. Anisotropic poroelasticity. III

Biot's equations in the diffusive range:

$$\nabla \cdot \sigma(u) = 0,$$
$$\mathrm{i}\omega \frac{\eta}{\kappa} u^f(x,\omega) + \nabla p_f(u) = 0,$$

$\omega = 2\pi f$: **angular frequency**

η: **fluid viscosity** κ: **frame permeability**

The Mesoscale. Anisotropic poroelasticity. IV

τ_{ij}: stress tensor of the equivalent VTI medium

For a closed system($\nabla \cdot u^f = 0$), the corresponding stress-strain relations, stated in the space-frequency domain, are

$$
\begin{aligned}
\tau_{11}(u) &= p_{11}\ \epsilon_{11}(u^s) + p_{12}\ \epsilon_{22}(u^s) + p_{13}\ \epsilon_{33}(u^s),\\
\tau_{22}(u) &= p_{12}\ \epsilon_{11}(u^s) + p_{11}\ \epsilon_{22}(u^s) + p_{13}\ \epsilon_{33}(u^s),\\
\tau_{33}(u) &= p_{13}\ \epsilon_{11}(u^s) + p_{13}\ \epsilon_{22}(u^s) + p_{33}\ \epsilon_{33}(u^s),\\
\tau_{23}(u) &= 2\ p_{55}\ \epsilon_{23}(u^s),\\
\tau_{13}(u) &= 2\ p_{55}\ \epsilon_{13}(u^s),\\
\tau_{12}(u) &= 2\ p_{66}\ \epsilon_{12}(u^s).
\end{aligned}
$$

This approach provides the complex velocities of the fast modes and takes into account interlayer flow effects.

The experiments to determine the five p_{IJ} VTI stiffness

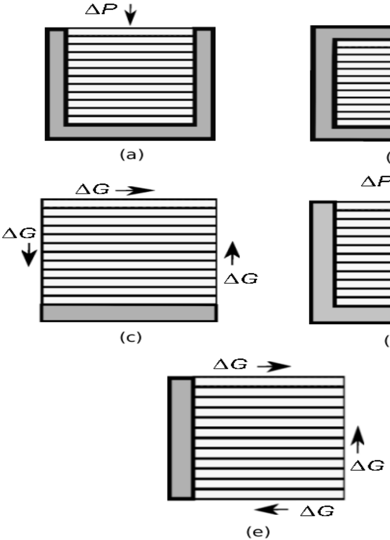

(I) : Figs (a) and (b) show how to determine p_{33} and p_{11}, (c) determines p_{55}, (e) determines p_{66} and (d) determines p_{13}.

Local degrees of freedom for the FEM solution of the harmonic tests.

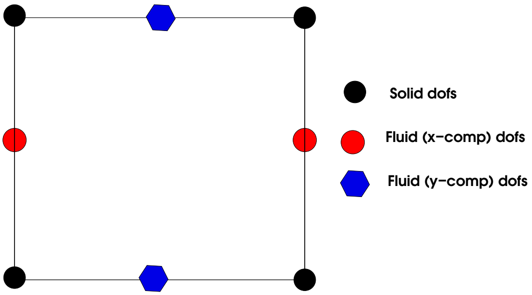

The solution of the oscillatory tests was computed using the FEM. The figure displays the local degrees of freedom (DOFs) associated with each component of the solid displacement and the fluid displacement vectors.

Numerical Experiments. I

Consider the following cases for a square poroelastic sample of 160 cm side length and 10 periods of 1 cm fracture, 15 cm background:

- Case 1: A brine-saturated sample with fractures.
- Case 2: A brine-CO_2 patchy saturated sample without fractures.
- Case 3: A brine-CO_2 patchy saturated sample with fractures.
- Case 4: A brine saturated sample with a fractal frame and fractures.

The complex stiffnesses $p_{IJ}(\omega)$ were determined for 30 frequencies using a public domain sparse matrix solver.
The $p_{IJ}(\omega)$'s determine the energy velocities and dissipation coefficients shown in the next figures.

Polar representation of energy velocity vector of qP waves at 50 Hz for Cases 1, 2 and 3

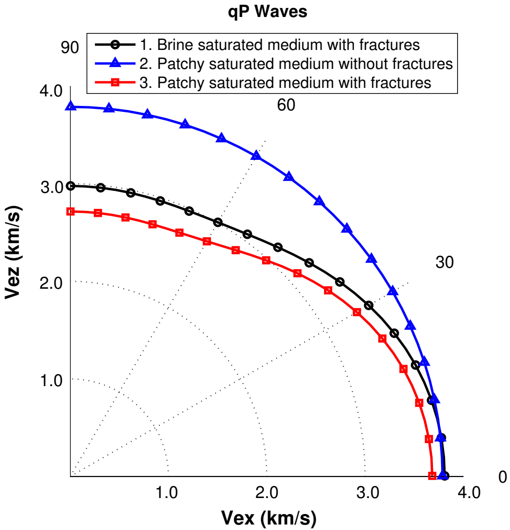

Cases 1 and 3 show velocity anisotropy caused by fractures. Case 3 (patchy saturation) exhibits lower velocities. Velocity behaves isotropically in Case 2.

Polar representation of dissipation factor of qP waves at 50 Hz for Cases 1, 2 and 3

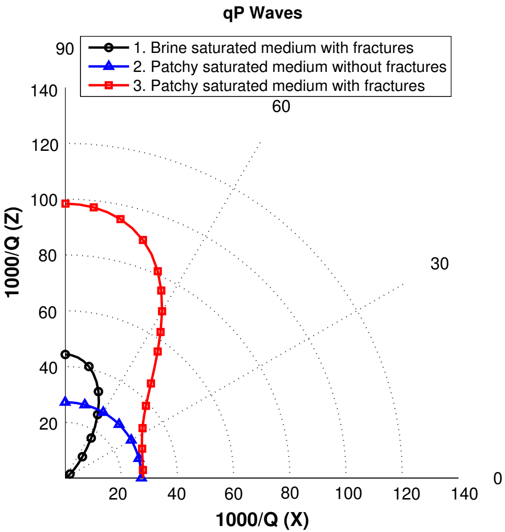

Fractures induce strong Q anisotropy for angles normal to the fracture plane, enhanced by patchy saturation.

Fluid pressure distribution at 50 Hz. Compressibility test for p_{33} for Case 3.

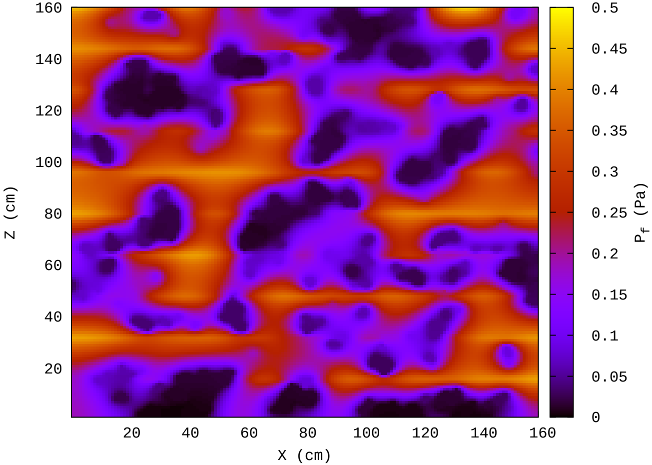

Compression is normal to the fracture plane. This Figure illustrates the mesoscopic loss effect.

Polar representation of energy velocity vector of qSV waves at 50 Hz for Cases 1, 2 and 3

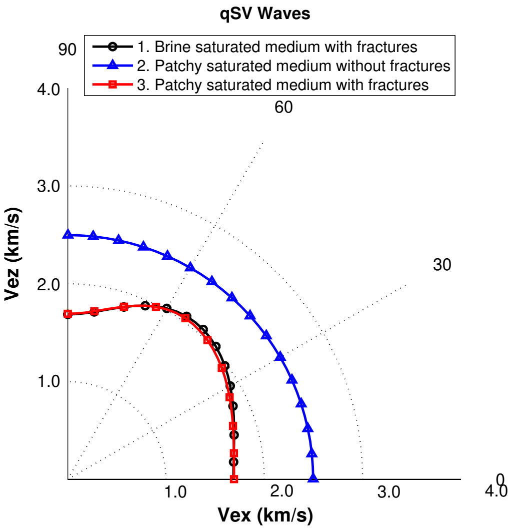

Velocity anisotropy is induced by fractures (Cases 1 and 3). Patchy saturation does not affect the anisotropic behavior of qSV velocities. Case 2 is isotropic with higher velocity values than for the fractured cases.

Polar representation of dissipation factor of qSV waves at 50 Hz for Cases 1, 2 and 3

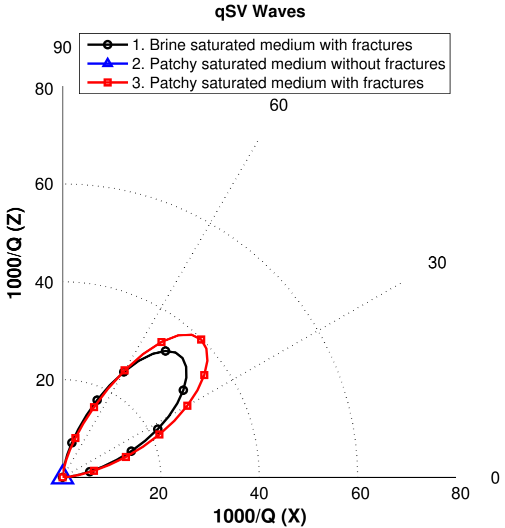

qSV attenuation anisotropy is strong for angles between 30 and 60 degrees. The lossless Case 2 is represented by a triangle at the origin.

Polar representation of energy velocity of SH waves at 50 Hz for Cases 1, 2 and 3

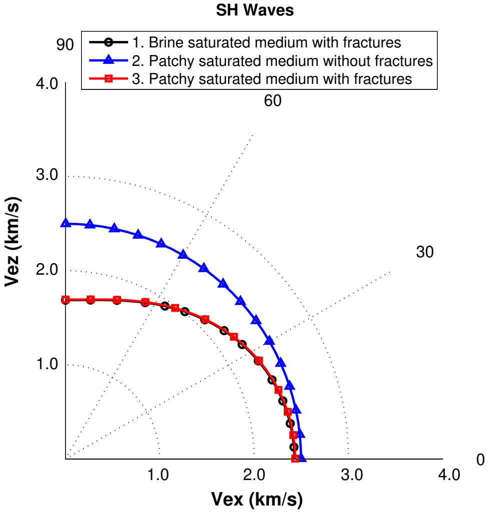

SH velocity anisotropy is induced by fractures. (Cases 1 and 3). Velocity for Case 2 is isotropic. SH waves are lossles since p_{55} and p_{66} are real.

Lamé coefficient (GPa) for the brine-saturated fractal porosity-permeability sample of Case 4.

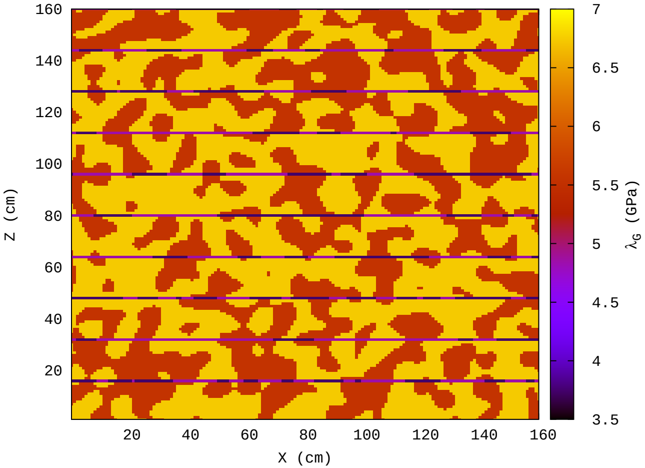

log $\kappa(x,z) = \langle$**log** $\kappa\rangle + f(x,z)$, $f(x,z)$**: fractal representing the spatial fluctuation of the permeability field** $\kappa(x,z)$**.**

Polar representation of energy velocity vector of qP waves at 50 Hz for Cases 1 and 4.

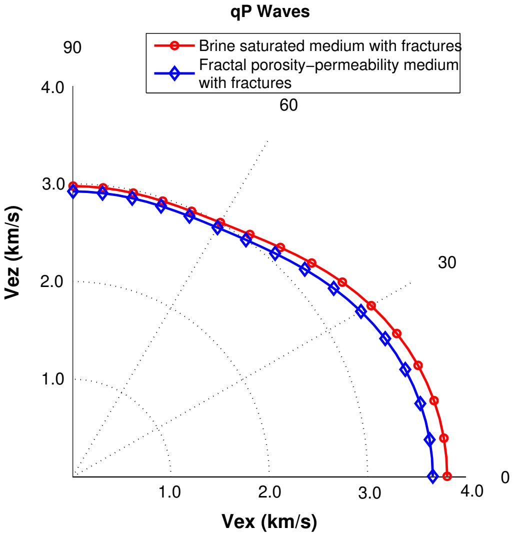

Note the decrease in velocity of qP waves for angles normal to the fracture plane.

Polar representation of dissipation factor of qP waves at 50 Hz for Cases 1 and 4.

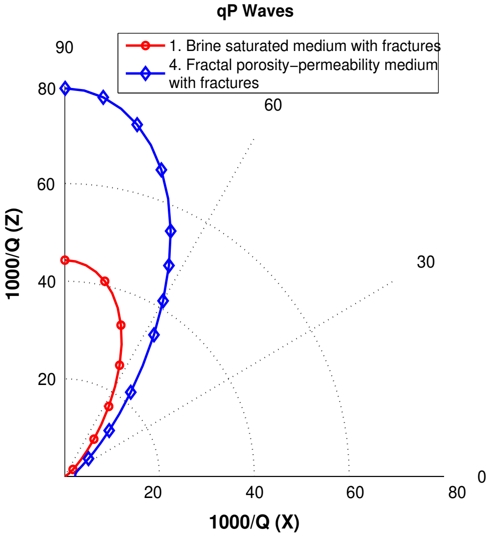

Note the increase in Q anisotropy of qP waves for angles normal to the fracture plane.

Polar representation of energy velocity vector of qSV waves at 50 Hz for Cases 1 and 4.

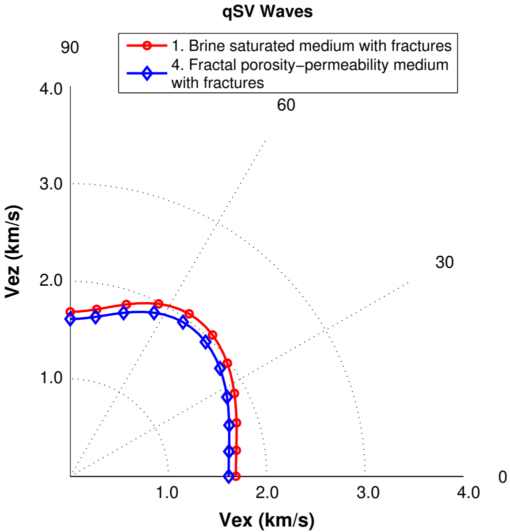

There is decrease in qSV velocity for Case 4

Polar representation ofdissipation factor of qSV waves at 50 Hz for Cases 1 and 4.

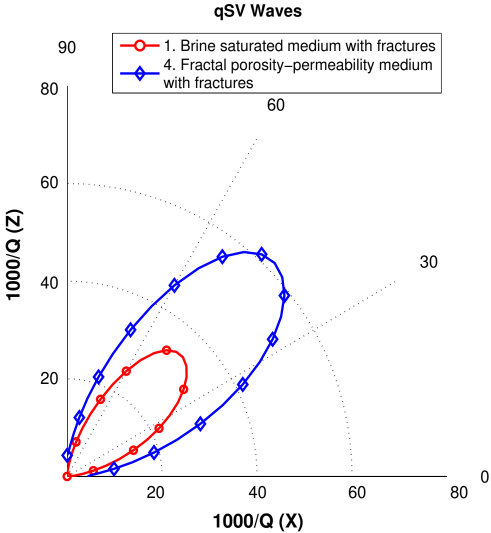

Attenuation of qSV waves is strong for angles between 30 and 60 degrees, and higher in Case 4.

The Macroscale I. Seismic modeling

We solve the following boundary value problem at the macroscale in a domain Ω with boundary $\partial\Omega$:

$$\begin{aligned} \omega^2 \rho u + \nabla \cdot \tau(u) &= F, \quad \Omega \\ -\tau(u)\nu &= i\omega\mathcal{D}u, \quad \partial\Omega, (\text{absorbing B. C., } D > 0) \end{aligned}$$

$u = (u_x, u_z)$: macroscopic displacement vector, ρ: average density.
$\tau(u)$: stress-tensor of our equivalent VTI medium, defined in terms of the $p'_{IJ}s$.

The solution of the above wave equation was computed at a range of frequencies of interest using an iterative FE domain decomposition procedure.

The Macroscale Model. I

- The macroscopic model consists of an isotropic square background Ω of 1.6 km side length containing an anisotropic layer of 400m thickness of either horizontal or vertical aligned fractures (HTI or VTI medium).
- The stiffnesses coefficients of the anisotropic layer are those determined using the harmonic experiments, for the cases of fully brine saturated fractures (Case 1) or 10 % patchy CO_2 saturation (Case 3).
- The isotropic background has P- and S-wave velocities at 50 Hz equal to 2633 m/s and 1270 m/s, respectively.

The Macroscale Model. II

- For the HTI-case, qP- and qSV-wave velocities at 50 Hz are equal to 3808. m/s and 1686 m/s, respectively, while for the VTI-case qP- and qSV-wave velocities at 50 Hz are equal to 3008. m/s and 1686 m/s, respectively
- The computational mesh consists of square cells having side length 4 m, and The source is a dilatational perturbation of central frequency is 50 Hz, located at $(x = 800m, z = 6.m)$.

The macroscopic model. III

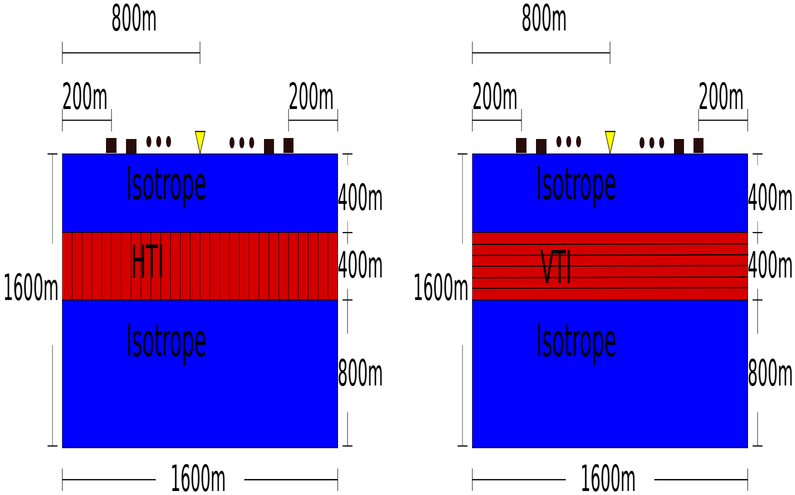

Snapshots of z-component of velocity at 280ms (left) and 300 ms (right). HTI brine saturated fractures.

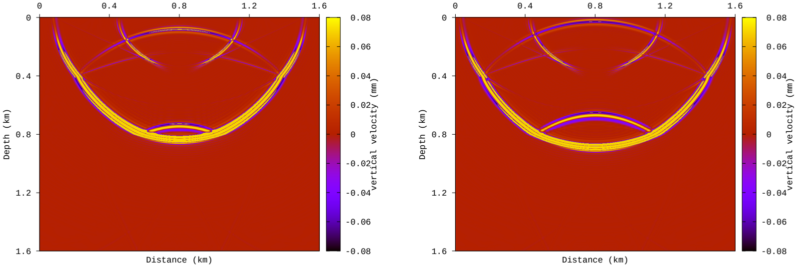

At 280 and 300 ms we can observe an upgoing P-wavefront and a tiny upgoing S-wavefront reflected at the top of the HTI layer and an upgoing qP-wavefront generated by reflection of the downgoing qP-wave at the bottom of the HTI layer. At 300 ms the reflected P-wave generated at the top of the HTI layer is arriving at the surface geophones.

Synthetic traces. HTI and VTI brine saturated fractures.

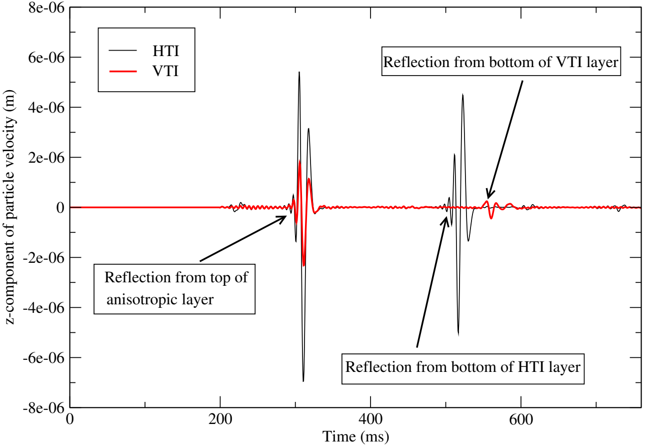

Synthetic traces. HTI brine and patchy brine-CO_2 saturated fractures.

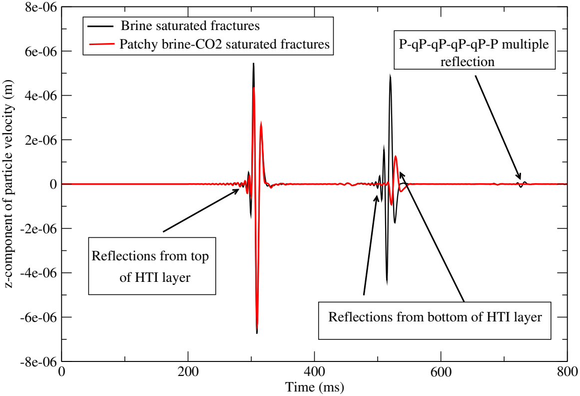

Synthetic seismograms. HTI (left) and VTI (right) brine saturated fractures.

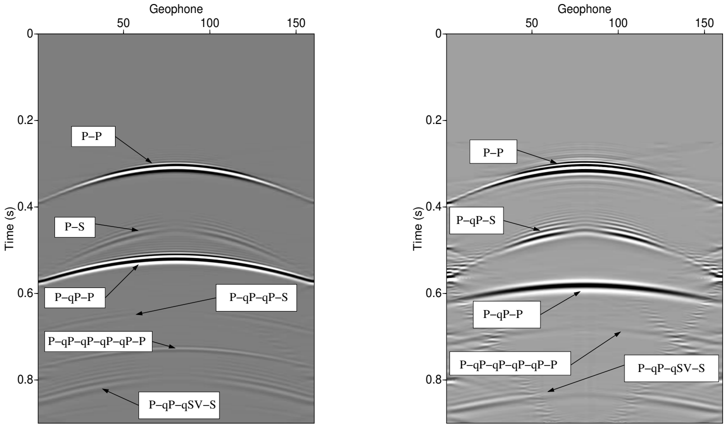

The seismograms show the arrivals of P and S waves reflected at the top of the HTI and VTI layers, and later arrivals from conversions from incident P to qP and qSV waves at the top and bottom of the layers. It is clearly seen the late P-qP-P arrival of the VTI case as compared with the corresponding one in the HTI case. qP-velocities in the HTI and VTI layers are about 3800 m/s and 3000m/s, respectively.

Synthetic seismograms. HTI brine (left) and 10 % CO_2 (right) saturated fractures.

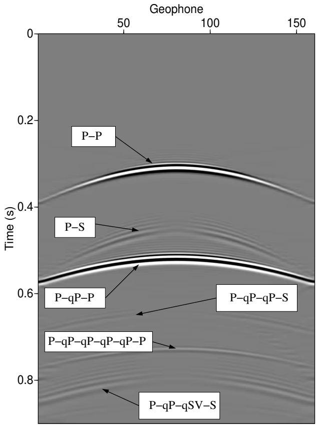

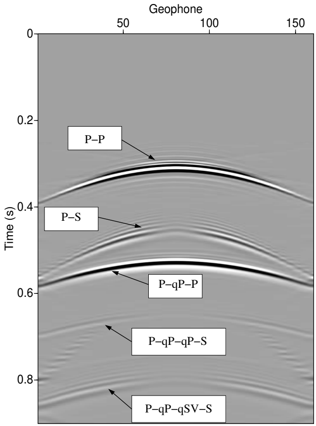

Seismograms show arrivals of P and S waves reflected at the top of the HTI layer, and later arrivals corresponding to conversions from incident P to qP and qSV waves at the top and bottom of the layer. Note that the P-qP-qP-qP-qP-P arrival in the brine-saturated case is not seen in the patchy brine-CO_2 case (strong attenuation $Qp \approx 10$ at normal incidence). Instead qSV-waves are less attenuated when CO_2 is present and the P-qP-qSV-S-arrival is still observed.

Conclusions

- Numerical upscaling procedures allow to represent at the macroscale anisotropy induced by a dense set of aligned fractures at mesoscopic scales in fluid-saturated poroelastic samples.
- The Finite Element Method is a useful tool to solve local problems at the mesoscale in the context of Numerical Rock Physics and global wave propagation problems at the macroscale.
- The techniques presented here to model acoustics of porous media in Geophysics can be extended to other fields, like ultrasound testing of quality of foods, groundwater flow and contamination among others
- Thanks for your attention !!!!!.